RApid Blade and Blade-Vortex InTeraction (RABBIT) Reimagined: Algorithm Improvement and User-Friendly Interface Implementation

Natasha L. Schatzman
Aerospace Engineer
NASA Ames Research Center
Moffett Field, CA, USA

Kevin Holly
Senior Application Engineer
MathWorks
Chevy Chase, MD, USA

ABSTRACT

Rotorcraft noise source identification and reduction is crucial to the emergence of the Urban Air Mobility (UAM) market. One key rotor noise source is Blade Vortex Interaction (BVI), caused by the rotor blades interacting with the rotor wake. The low-fidelity RApid Blade and Blade-Vortex InTeraction (RABBIT) tool was created to predict the location and characteristics of BVI noise. RABBIT enables engineers to quickly design and simulate UAM configurations and understand BVI occurrences for a desired flight condition. Furthermore, RABBIT can also identify the time and location of blade overlap for coaxial rotors. RABBIT is not a general acoustic prediction tool, but instead utilizes vortex and wake parameters to visualize and predict BVI aerodynamics. RABBIT algorithm has been further developed including reduction of computational time, accounting for BVI source time arrival, improved vortex strength modeling, and BVI impulse factor. A user-friendly app is presented with the intent of bringing RABBIT to the masses to allow engineers from various educational backgrounds to design and begin to understand BVI. Furthermore, RABBIT capabilities are highlighted by a parameter study highlighting key parameters that impact BVI along with highlighting RABBIT's ability to identify BVI occurrences from other rotors.

NOTATION

A	Rotor area (ft^2)
a_o	Speed of sound (ft/s)
c	Chord (ft)
$c_{l\alpha}$	2D lift curve slope (2π/rad)
C_T	Rotor balance thrust coefficient $\left(\frac{T}{\rho A(\Omega R)^2}\right)$
D	Distance from rotor source to observer (ft)
F	Blade loading (lb/in)
h	Blade vortex miss distance (ft)
$\bar{I}$	Impulse factor
M_{tip}	Rotor hover tip Mach number
M_{tr}	Mach trace number
N_b	Number of blades
o	Rotor observer location
P	Acoustic pressure (Pa)
R	Rotor radius (ft)
RPM	Rotor rotational speed (rev/min)
s	Rotor source location
T	Thrust (lbs.)
TOL	Tolerance factor (%)
t	Observer time (s)
V_b	Translating blade velocity (ft/s)
V_∞	Forward flight velocity (ft/s)
X	Streamwise coordinate relative to rotor 1 hub center (positive into the wind) (ft)
Y	Vertical coordinate relative to rotor 1 hub center (positive down) (ft)
Z	Lateral coordinate relative to rotor 1 hub center (ft)
α_{TPP}	Rotor tip path plane angle, positive tilting forward (deg)
β_0	Rotor coning angle (deg)
γ	Blade vortex interaction angle (deg)
$\Delta\Psi_w$	Wake age resolution (deg)
λ_0	Inflow ratio
μ	Advance ratio $\left(\frac{V_\infty}{\Omega \cdot R}\right)$
Γ	Vortex strength, (ft^2/s)
$\bar{\Gamma}_s$	Vortex strength factor $\left(\frac{\Gamma}{2\pi h V_b}\right)$
ρ	Air density (slug/ft^3)
σ	Rotor solidity $\left(\frac{N_b c}{\pi R}\right)$
τ	Source time (s)
Φ	Blade phase angle (deg)
χ	Wake skew angle (deg)
Ψ	Azimuth angle (deg)
Ψ_b	Hit blade azimuth angle location (deg)
Ψ_s	Blade vortex source blade azimuth angle location (deg)
Ψ_w	Wake age (deg)
Ω	Rotor angular speed (rad/s)

INTRODUCTION

With the emergence of the Urban Air Mobility (UAM) market, identifying and reducing the source of rotorcraft noise becomes critical for human acceptance, especially when operating in populated areas. One of the main sources of noise during takeoff and landing is Blade Vortex Interaction (BVI), which is caused by the rotor blades interacting with the rotor wake. Being able to predict such acoustic phenomena is

Presented at the VFS 6th Decennial Aeromechanics Specialists' Conference, Santa Clara, CA, USA Feb. 6-8, 2024.

critical in the design process of UAM vehicles. In result, NASA's Revolutionary Vertical Lift Technology (RVLT) project emphasizes the importance of having versatile prediction tools to support the prediction of rotorcraft acoustics. The current toolchain workflow that enables the prediction of rotor noise includes calculating loads from Comprehensive Analytical Model of Rotorcraft Aerodynamics and Dynamics II (CAMRAD II) (Ref. 1) to feed into the Aircraft NOise Prediction Program 2 (ANOPP2) and the AeroAcoustic ROtor Noise (AARON) system (Ref. 2). Due to the computationally expensive and time-consuming nature of these programs, a rapid and lower fidelity tool was created by Schatzman (Ref. 3). The RApid Blade and Blade-Vortex InTeraction (RABBIT) tool was created to predict the location and description of Blade-Vortex Interaction (BVI) on a rotor disk.

BACKGROUND

In 1995, Sim and George (Ref. 4) developed a program using Beddoes' prescribed wake model (Ref. 5) to resolve blade-vortex interaction events which included a new method to evaluate and quantify BVI in terms of blade loading (F). Sim and George used the Beddoes prescribed wake model to model the wake generated from the blade tip to predict a variety of important BVI factors. Beddoes' prescribed wake model uses parameters including radius (R), advance ratio (μ), wake skew angle (χ), inflow (λ_0), blade position (Ψ_b), and wake age (Ψ_w). Major BVI factors can be summarized into vortex strength factor ($\bar{\Gamma}_s$), BVI Impulse ($\bar{I}$), BVI impulse function, and blade airfoil aerodynamic factors as shown in

Equation 1. These factors can be rearranged to calculate $\partial F/\partial t$. Within these factors the following parameters are identified as key components: vortex strength (Γ), translating blade velocity (V_b), vortex miss distance (h), BVI interaction angle (γ), blade hit azimuth angle location (Ψ_b), location of blade vortex source azimuth location (Ψ_s), and rotor angular speed (Ω). Furthermore, key geometrical properties include 2D lift curve slope (c_{l_α}) and chord (c). To better visualize some of these key BVI intensity parameters, the translating blade velocity, miss distance, blade vortex interaction angle, vortex wake age (Ψ_w) are depicted in Fig. 1 a) through d), respectively. The current version of RABBIT does not account for trace Mach number, which is an important parameter for radiation cone noise dependent on blade vortex interaction angle as studied by Ringler and George (Ref. 6).

Equation 1

BVI Impulse ($\bar{I}$)

Blade airfoil factors

$$F = \left(c_{l_\alpha} c\right)\left(\frac{1}{2}\rho V_b^2\right)\left(\frac{\Gamma}{2\pi V_b h}\right)\left(\frac{V_b \cos\gamma}{h}\right)\left(\frac{1-\left(\bar{I}\frac{(\Psi_b-\Psi_s)}{\Omega}\right)^2}{\left(1+\left(\bar{I}\frac{(\Psi_b-\Psi_s)}{\Omega}\right)^2\right)^2}\right)$$

vortex strength factor ($\bar{\Gamma}_s$)

BVI impulse function

The initial RABBIT code could predict and visualize blade crossing locations and BVI impulse factor for single and coaxial rotors (Ref. 3), and was validated against a single rotor blade from Sim (Ref. 4). RABBIT was further validated by using the NASA Revolutionary Vertical Lift Technology (RVLT) concept vehicles (Quiet Single Main Rotor (QSMR), Side-by-Side, and Quadrotor) (Ref. 7). Each concept vehicle was first modeled with CAMRAD II to see the differences between the prescribed wake used in RABBIT and the free wake computed by CAMRAD II. To validate BVI intensity, the acoustics tool ANOPP2 was used to compare the BVI locations and amplitudes with acoustic pressure time history (Ref. 8). It was suggested by Sim and George (Ref. 4) to use a vortex core of 0.5% of the chord. Due to this suggestion, a tolerance factor was implemented to allow the specification of how close a vortex must be to be considered an 'interaction.' This allows the user to specify how strong of a BVI they wish to consider, see Fig. 2. The tolerance factor is based on the percentage of the chord. If a vortex element is identified to be within the blade area with tolerance factor applied, then BVI parameters are calculated.

a)

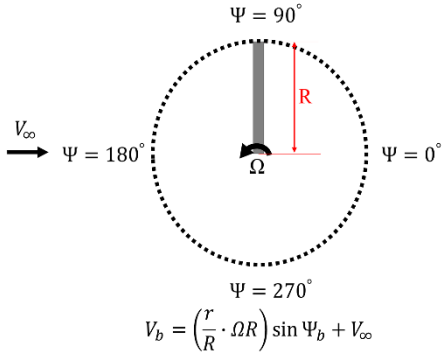

b)

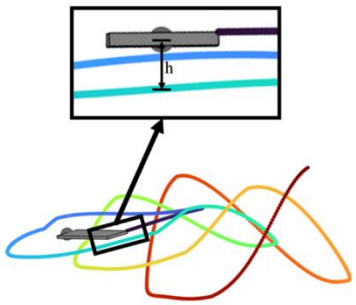

c)

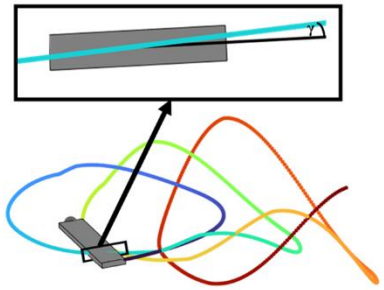

d)

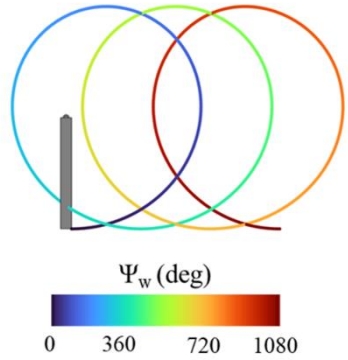

Figure 1. Visual representation of a) translating blade velocity (V_b), b) miss distance (h), c) blade vortex interaction angle (γ), and d) vortex wake age (Ψ_w).

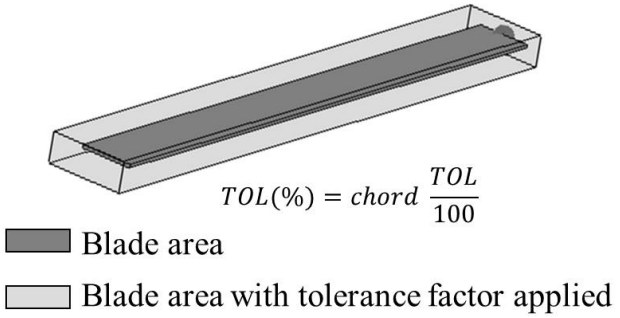

Figure 2. RABBIT tolerance factor graphical representation and equation.

ALGORITHM IMPROVEMENT AND COMPARISON

RABBIT's algorithm has been further improved by means of decreasing computational time, accounting for BVI source time arrival consideration, improved vortex strength modeling, and improved BVI impulse factor. To aid in highlighting RABBIT's algorithm improvements the Lopes rotor was selected due to its simple geometry. The Lopes rotor geometry and observer location is provided in Table 1, while RABBIT specific input parameters are found in Table 2.

For each some cases presented, RABBIT results are compared to CAMRAD II and ANOPP2 (Ref. 9) simulations. The Lopes rotor was modeled in CAMRAD II as a rigid rotor using a free wake to capture BVI occurrences. In ANOPP2, to ensure BVI noise was captured, a microphone was modeled at an elevation of 45 degrees down from the center of the rotor plane in the far field 10R away. Acoustic time history was filtered to only include the 10th through the 50th blade pass frequency to remove non-BVI noise sources.

RABBIT does not compute acoustic pressure, so validation against CAMRAD II and ANOPP2 is performed by comparing RABBIT's blade loading to the acoustic pressure computed by CAMRAD II and ANOPP2.

Table 1. Lopes rotor geometry and observer location.

Parameter	Value
Number of rotors	1
Number of blades	4
Rotor radius (ft)	32.808
Chord (ft)	1.6404
Blade phase (deg)	0, 90, 180, 270
Airfoil	NACA0012
Observer (X_o, Y_o, Z_o)	10 R, 0 R, -10 R

Table 2. RABBIT input parameters for Lopes rotor simulation.

Parameter	Value
Time step (deg)	1
Revolutions	0.25
Ψ_w (deg)	1440
$\Delta\Psi_w$ (deg)	1
BVI TOL (%)	15

Computational Time

The performance of the RABBIT algorithm has been significantly enhanced through an optimization process. Using the MATLAB Profiler, critical bottlenecks in the code were identified and addressed (Ref. 10). Pre-allocation of vectors were introduced to minimize computational overhead. Previous nested 'for' loops were optimized by extricating independent operations, thereby reducing the number of variables iterated. Schemas comprising of cell arrays, structural arrays, and table arrays to store rotor information with greater efficiency were also introduced. These schemas not only streamline the code by eliminating the need for hardcoding each rotor, but also contributed to a reduction in both the number of variables and the overall lines of code. As a result of these cumulative enhancements, a substantial decrease in runtime was achieved, with the optimized algorithm performing twenty times faster than its predecessor.

BVI Source Arrival Time

Validation of this effort is shown in Fig. 3, where a) uses source time (τ) for RABBIT and b) accounts for arrival time to the microphone location. Microphone location was considered by identifying source time (τ) and location (X_s, Y_s, Z_s), and observer time (t) and location (X_o, Y_o, Z_o) within RABBIT. The time at which a BVI event occurs is the source time. However, because these BVI events can occur anywhere on the rotor disk and the speed of sound (a_o) is constant, the effect of events with the same source time may not arrive at an observer (microphone) at the same time due to difference in distance (D) to the observer. Previously, RABBIT did not account for observer time. The current RABBIT algorithm corrects for observer arrival time as described in Equation 2 for a given microphone location.

Figure 3 shows RABBIT's blade loading using source time and observer time. If source time is only accounted for (Fig. 3 a) BVI occurrences are clustered around 15, 30, 50 and 80-degrees azimuth. Accounting for observer location (Fig. 3 b) places BVI occurrences at 15, 45, 70, and 85 degrees. RABBIT identified the largest BVI occurrence at 45 degrees, which is similar to CAMRAD II + ANOPP2's prediction of a large BVI occurrence also at 45 degrees azimuth.

Equation 2

$$X = X_o + X_s, \quad Y = Y_o + Y_s, \quad Z = Z_o - Z_s$$

$$D = \sqrt{X^2 + Y^2 + Z^2}$$

$$t = \frac{D}{a_o} + \tau$$

a)

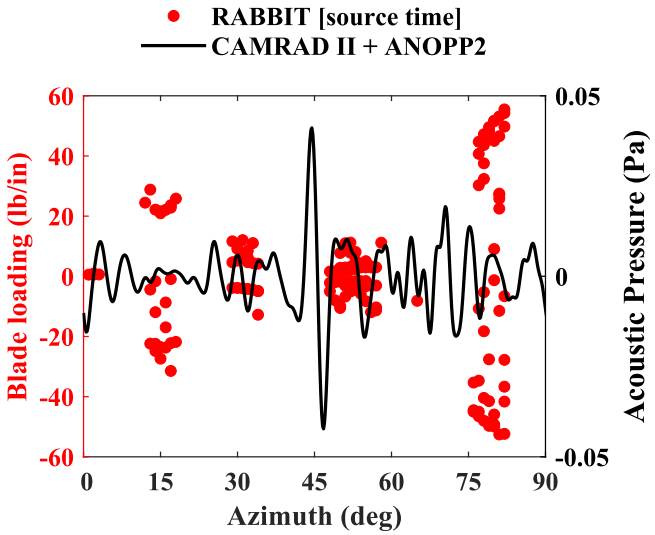

b)

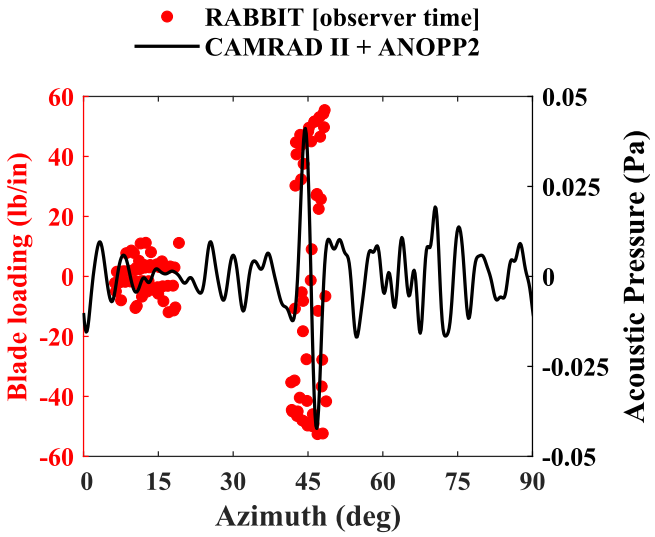

Figure 3. RABBIT and CAMRAD II + ANOPP2 predictions for a) without and b) with improved observer time shift (Lopes rotor: RPM = 227, μ = 0.10, α_{TPP} = 5 deg, C_T = 0.005).

Vortex Strength Modeling

Previously, RABBIT did not account for change in vortex strength (Γ), though it is known that rotor vortex strength is dependent on rotor performance and geometrical properties (Ref. 4). Due to RABBIT's past inability to account for vortex strength, RABBIT has been upgraded by calculating a vortex strength by accounting for rotational angular speed, radius, chord, and thrust, see Equation 3 (from Ref. 11). This simplified vortex strength approximation was developed for an "ideal" rotor operating in hover. It is suggested that a more

accurate model be implemented at a future time to include forward velocity to predict vortex strength more actually.

Figure 4 shows RABBIT and CAMRAD II + ANOPP2 predictions for two blade loading conditions of 0.005 and 0.008 to highlight the importance of accounting for vortex strength (the contribution of the vortex strength to the loading derivative can be seen in Eq.1). A constant vortex strength of 100 ft^2/s was previously used within RABBIT and is shown in blue. Results from CAMRAD II + ANOPP2 show a large change in acoustic amplitude as blade loading increases, whereas RABBIT's blade loading only sees a small change in blade loading for a constant vortex strength of 100 ft^2/s. For each blade loading case the maximum and minimum peaks are identified, and the delta difference is reported for the constant vortex of 100 ft^2/s and improved vortex model. The improved vortex model resulted in the ability to better report BVI intensity and resulted in a significant difference in peak-to-peak blade loading.

Equation 3

$$\Gamma = 2\Omega Rc\left(\frac{C_T}{\sigma}\right)$$

a)

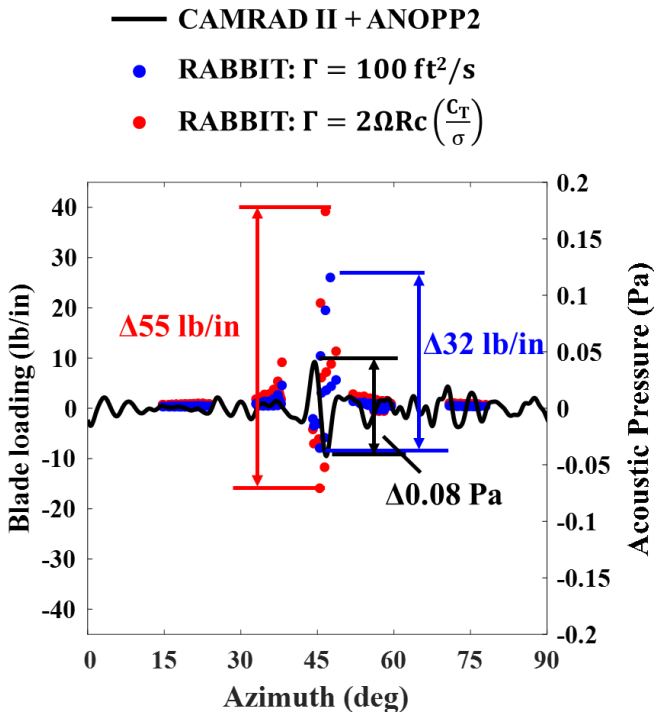

b)

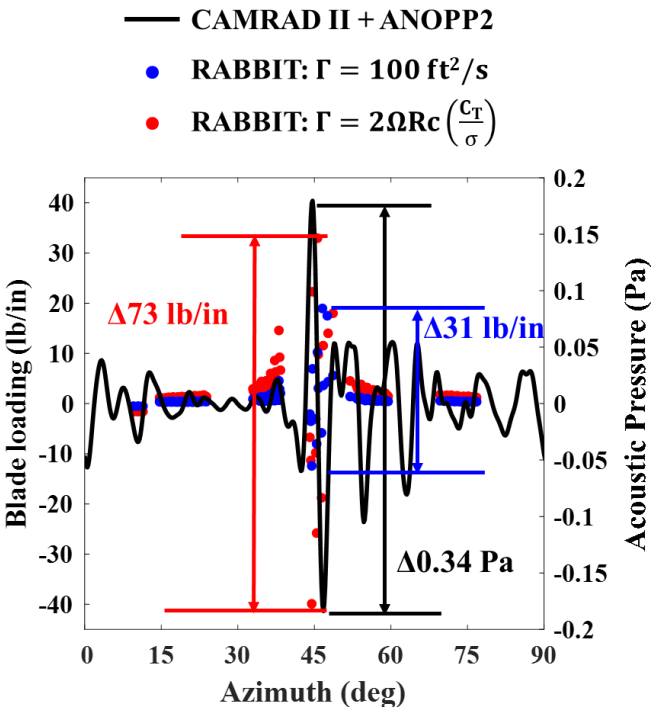

Figure 4. RABBIT and CAMRAD II + ANOPP2 predictions comparing a) C_T = 0.005 and b) C_T = 0.008 for Lopes rotor with and without improved vortex strength modeling (Lopes rotor: RPM = 227, μ = 0.10, α_{TPP} = 5 deg).

RABBIT INPUT PARAMETER SENSITVITY STUDY

A study was conducted to analyze the sensitivity of several selected RABBIT input parameters, including number of revolutions of the rotor, Ψ_w (wake age), wake age resolution ($\Delta\Psi_w$), and TOL. A time step of 1 degree was chosen to match CAMRAD + ANOPP2 inputs. The Lopes rotor was used due to its simple geometry rotor consisting of four blades with no twist, constant chord, and a single airfoil, see Table 1 (Ref. 2).

Due to the rotational symmetry of the Lopes rotor, it is possible to reduce computational time from 126.07 seconds to 30.54 seconds by modeling only a quarter of a revolution. A study was performed for the Lopes rotor for equal blade phase angles (Φ) of 0, 90, 180, 270 degrees and for an unequal blade phase angles of 0, 15, 200, 330 degrees, see Fig. 5 a) and b) respectively. Results from this study reveal a periodic pattern for equal blade phase angle spacing, therefore only a quarter of a revolution is needed for this case, whereas for unequal blade phase angles an entire revolution is needed to capture all possible BVI occurrences.

Failure to provide adequate wake age length could result in possible missed BVI instances, see Fig. 6 for with a comparison of wake lengths of a) 360, b) 720, and c) 1,440 degrees. Wake ages of 360 and 720 degrees fail to reach the

entirety of the rotor disk for this case and could result in not identifying possible BVI occurrences and could thus affect the predicted blade loading. It is important to note that wake age length will be dependent on rotor geometry and flight condition and that certain flight conditions may not need a wake length that covers the entirety of the rotor disk due to the wake being diverted away from rotor.

A wake age resolution of 1 degree ensured a precise modeling of Beddoes' wake model, which was previously validated against CAMRAD II's free wake for a single rotor resulting in capturing BVI occurrences between RABBIT and CAMRAD II's wake (Ref. 8). Variation of wake age resolution is shown in Fig. 7 for a resolution of a) 25, b) 5, and c) 1 degree. A wake resolution of 25 degrees compared to 1 degree fails to capture Beddoes' wake model characteristics above and below the rotor plane. A wake resolution of 5 degrees compared to 1 degree shows similar characteristics below rotor, but large differences above the rotor plane are not captured. The greater the wake resolution the more reduced wake fidelity and inaccurately predicted BVI.

A BVI hit tolerance of 5% was chosen by performing a BVI hit tolerance sensitivity and comparing tolerance factors of 1, 5, and 10% chord, see Fig. 8 for blade loading time history results against CAMRAD + ANOPP2 acoustic predictions. Results from this study reveal that with decreasing tolerance factor, a lesser number of BVI hit locations were identified. A tolerance factor of 1% was able to identify the strong BVI occurrence around 45 degrees, though failed to capture absolute maxima and minima as was achieved by using a tolerance factor of 5 and 10%. A tolerance factor of 5 and 10% also was able to identify several weaker BVI details in comparison to only 1%. Additional weaker BVI occurrences were identified by RABBIT, but not noticeable in the CAMRAD + ANOPP2 acoustic predictions. It was concluded that the additional BVI occurrences were from wake ages beyond 500 degrees azimuth. Wake age is not accounted for beyond 360 degrees in the current RABBIT algorithm.

a)

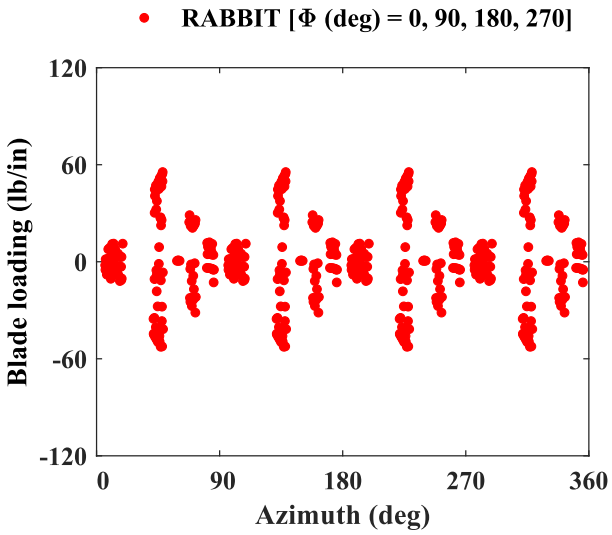

b)

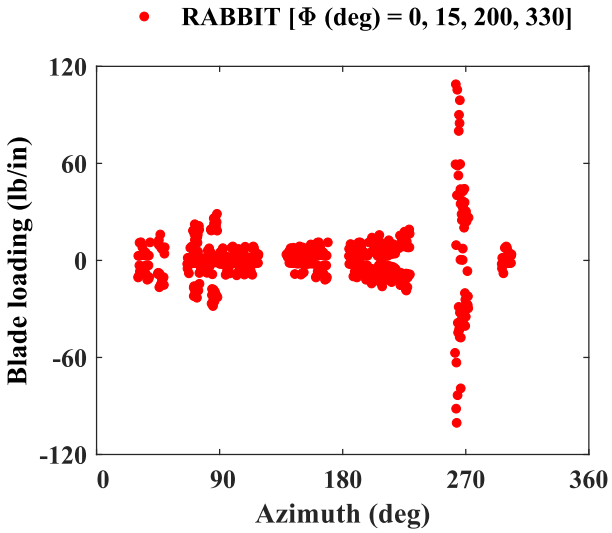

Figure 5. RABBIT simulation for a) equal and b) unequal blade phase angles (Lopes rotor: RPM = 227, μ = 0.1, α_{TPP} = 5 deg, C_T = 0.005).

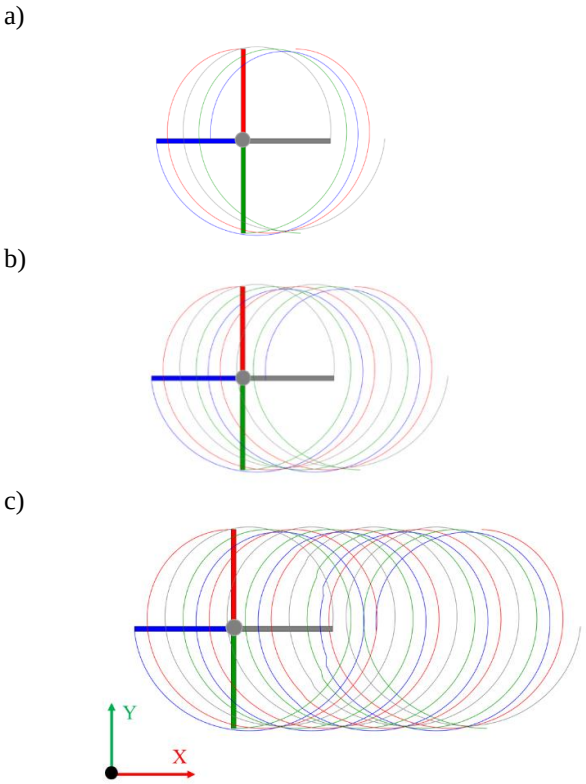

Figure 6. RABBIT simulation in X-Y plane for wake age lengths of a) 360, b) 720, and c) 1,440 degrees (Lopes rotor: RPM = 227, μ = 0.1, α_{TPP} = 5 deg, C_T = 0.005).

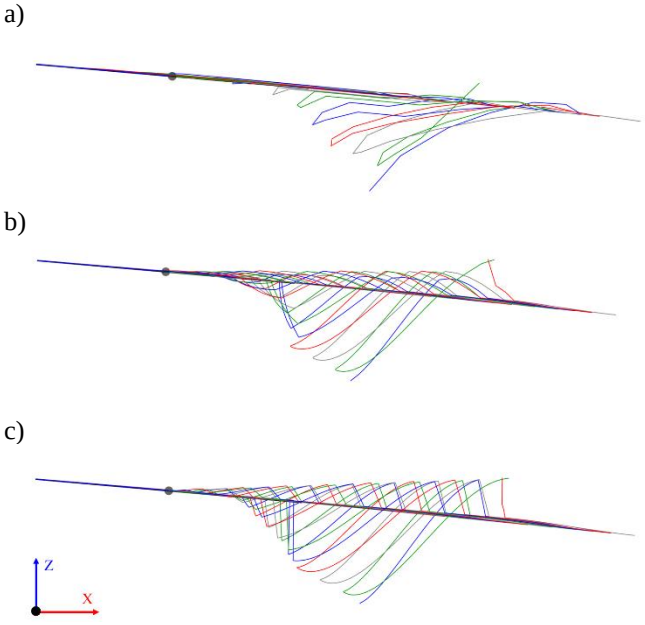

Figure 7. RABBIT simulation in X-Z plane for wake age resolutions of a) 25, b) 5, and c) 1 degree (Lopes rotor: RPM = 227, μ = 0.1, α_{TPP} = 5 deg, C_T = 0.005).

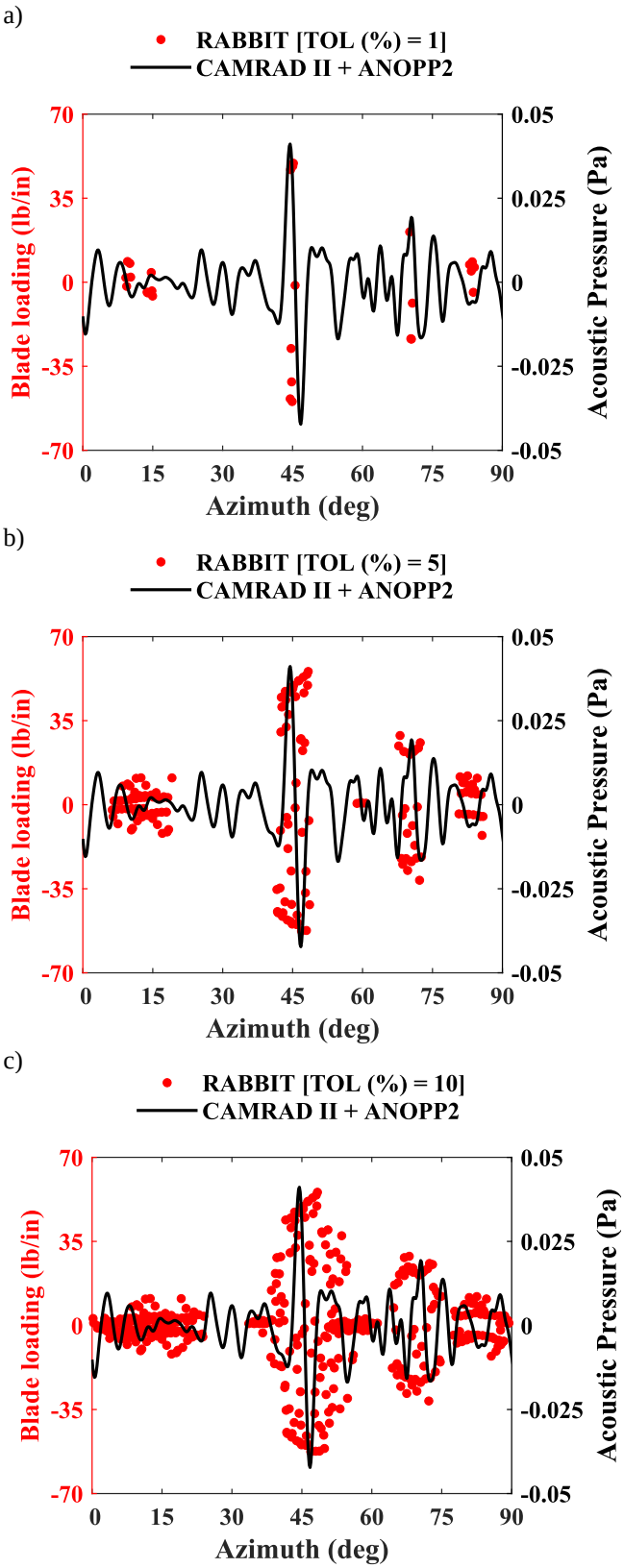

Figure 8. RABBIT tolerance factor sensitivity study for a) 1, b) 5, and c) 10% (Lopes rotor: RPM = 227, μ = 0.1, α_{TPP} = 5 deg, C_T = 0.005).

APP IMPLENTATION

RABBIT was originally written in the MATLAB environment as a script, which required the end user to be proficient in the MATLAB programming language. Due to this limitation, the RABBIT App was further developed using MATLAB's App Designer. The App Designer is an interactive development environment where the user can layout the visual components of a graphical user interface and program the app behavior with callback functions. The RABBIT App provides an easy-to-use interface that can be utilized without prior experience with MATLAB or, for that matter, rotorcraft acoustics (Ref. 10). Furthermore, RABBIT does not require users to have the MATLAB software to use as it was compiled to a standalone executable with MATLAB Compiler. The intent of developing the App was to bring RABBIT to the masses to allow engineers from various educational backgrounds to design and begin to understand BVI. Furthermore, an official logo for RABBIT was designed to make the tool aesthetically pleasing for a broad audience. The RABBIT logo is shown in Fig. 9, which entails the outline of a rabbit head, along with ears to simulate a four bladed single rotor.

The RABBIT App allows users to build and view rotor models in real time, with options to control blade chord, radius, unequal phasing, airfoil geometry, coning angle, location in space, and BVI tolerance. Furthermore, multiple rotors can be combined to create novel multi-rotor vehicles or fleets. A highlight of RABBIT's modeling capabilities is shown in Fig. 10.

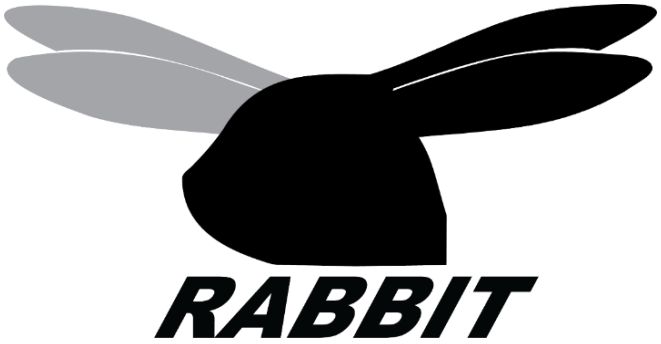

Figure 9. RABBIT logo.

a)

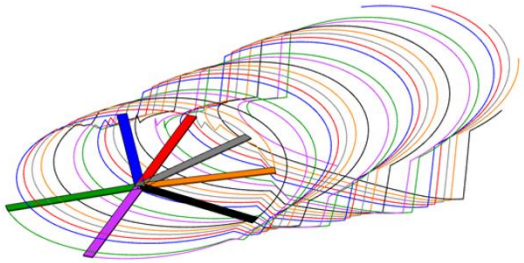

b)

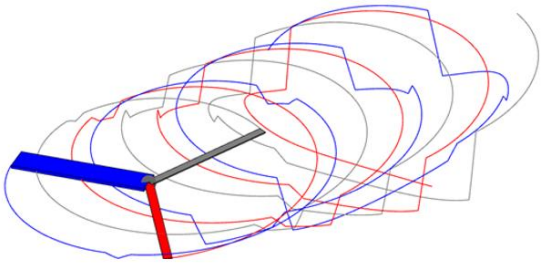

c)

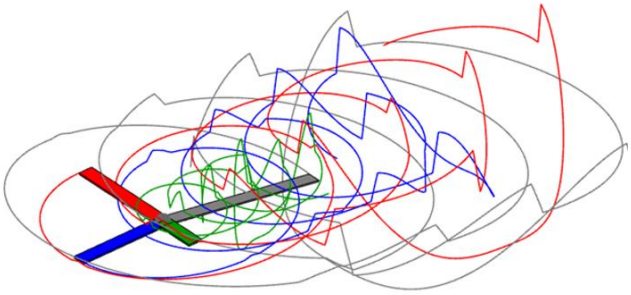

d)

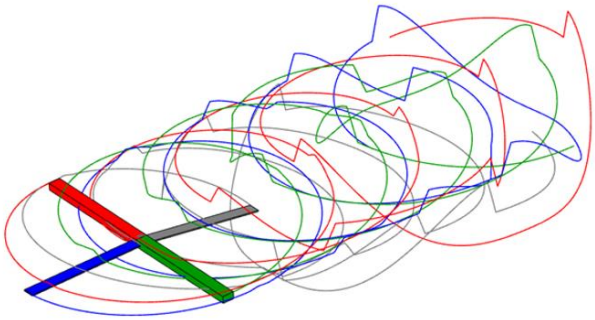

Figure 10. Example of RABBIT geometry modeling capabilities including a) unequal phasing and varying b) chord, c) radius, and d) coning angle per blade.

An example of RABBIT's user interface is shown in Fig. 11 for a quadrotor configuration. Interactive tables, sliding bars, and push buttons were implemented to allow engineers and designers to predict low-order acoustic impact of BVI occurrences. Furthermore, the design of the app implements the RABBIT logo with a background image consisting of the Atlanta skyline with NASA Urban Air Mobility (UAM) reference vehicles in flight, which improves users visual experience with the tool (Ref. 12).

The RABBIT App is designed to accommodate the simulation of an unrestricted number of rotors, with the only limitation being the available memory of the user's computer. Within the app's interface lies an intuitive table that houses all the necessary rotor parameters required for the simulation. Users have the flexibility to modify these values directly within the table, allowing for dynamic adjustments and customization of the simulation parameters to suit specific modeling needs. This feature enhances the app's versatility and user control. Required global vehicle inputs include vehicle name, forward flight velocity (V_∞), density (ρ), wake resolution ($\Delta\Psi_w$), number of revolutions, azimuthal time step, wake age length (Ψ_w), and if the user wants a vortex on all blades or only the first blade. For each rotor, requirements include name, rotational direction, number of blades, radius, chord, blade phasing, advance ratio (μ), RPM, alpha tip path plane angle (α_{TPP}), coning angle (β_0), coefficient of thrust (C_T), location (X, Y, Z), BVI hit tolerance factor, and symmetrical NACA airfoil. At this time, RABBIT is written using US customary units.

Once the vehicle configuration and flight conditions are defined, a window pops up to allow users to select what output files they desire, along with location of the output files, see Fig. 12. Output selections include vehicle description, BVI location and intensity plot, BVI hit information, and blade overlap information and plot (for coaxial rotors only). Options to export via Text File (TXT) format or Comma Separated Values (CSV) file are available to users. The produced output of the BVI location and its intensity plot, as well as blade overlap information and the corresponding plot are currently exported as a Portable Network Graphic (PNG).

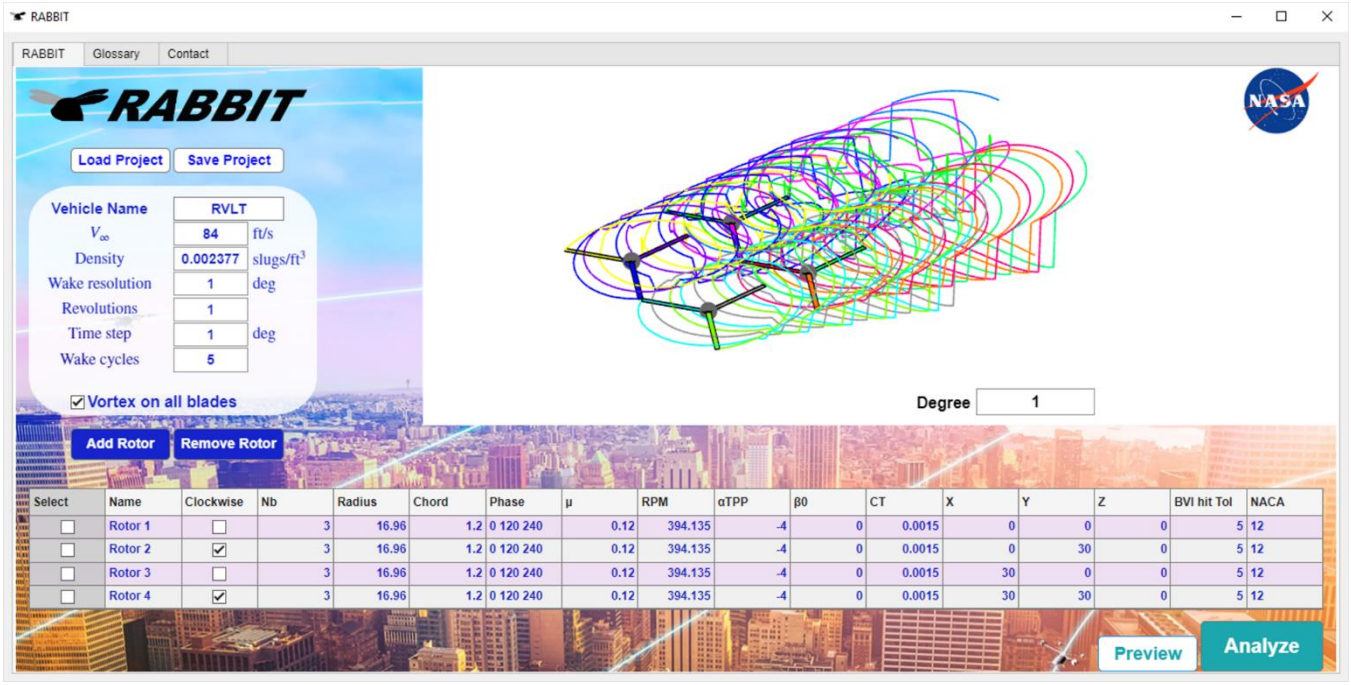

Figure 11. The RABBIT App's set-up GUI depicting a quadrotor configuration.

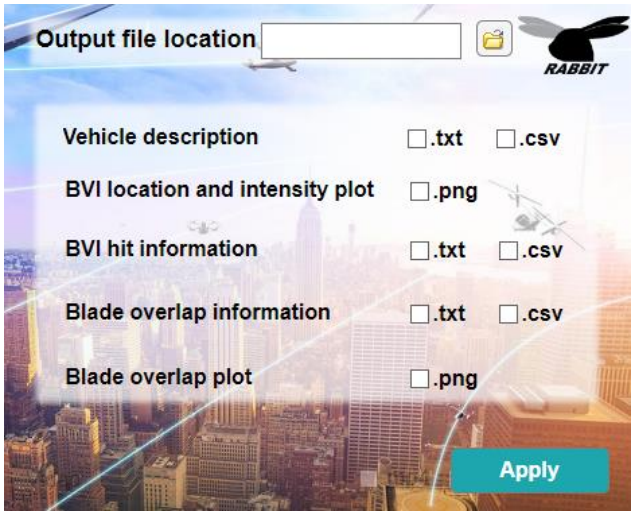

Figure 12. RABBIT output selection window.

RESULTS

To highlight improvements to RABBIT's algorithm, the NASA RVLT concept Quadrotor is validated and further analyzed to highlight RABBIT's capabilities to identify BVI occurrences from other rotors. See Table 3 and Table 4 for vehicle geometry, flight condition, and microphone position. RABBIT input parameters are provided in Table 4.

Table 3. NASA RVLT concept Quadrotor geometry and observer location.

Parameter	Value
Number of rotors	4
Number of blades	3
Rotor radius (ft)	9
Chord (ft)	0.75
Blade phase (deg)	0, 120, 240
Rear rotor height above front rotor	0.35 R
Tip speed (ft/s)	550
Coefficient of thrust (front rotors)	0.0063
Coefficient of thrust (rear rotors)	0.0058
Tip path plane (deg)	-2.5
Advance ratio	0.17
Observer (X_o, Y_o, Z_o)	10 R, 0 R, -15 R

Table 4. NASA RVLT concept Quadrotor input parameters for Lopes rotor simulation.

Parameter	Value
Time step (deg)	1
Revolutions	1
Ψ_w (deg)	1440
$\Delta\Psi_w$ (deg)	1
BVI TOL (%)	5

A visual rendering of the NASA RVLT concept Quadrotor is shown in Fig. 13 a) along with the b) RABBIT simulation in an isometrical view and c) the Y-Z plane with only front rotor wakes present to visualize possible rotor wake interactions from the front and rear rotors. Due to rotor height placement, no BVI occurrences coming from front rotors will occur, see Fig. 13 c). Results comparing RABBIT's blade loading CAMRAD II and ANNOP2 acoustic pressure for the RVLT Quadrotor reference vehicle are shown in Fig. 14. In general, RABBIT was able to identify strong BVI occurrences for this quadrotor case.

a)

b)

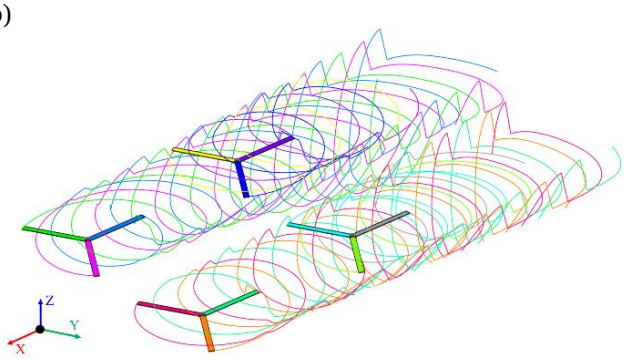

c)

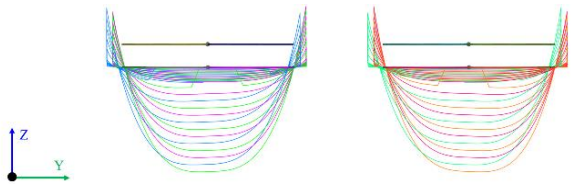

Figure 13. NASA RVLT Conceptual design quadrotor a) visual rendering and b) RABBIT simulation isometric view, and c) RABBIT simulation Y-Z plane view.

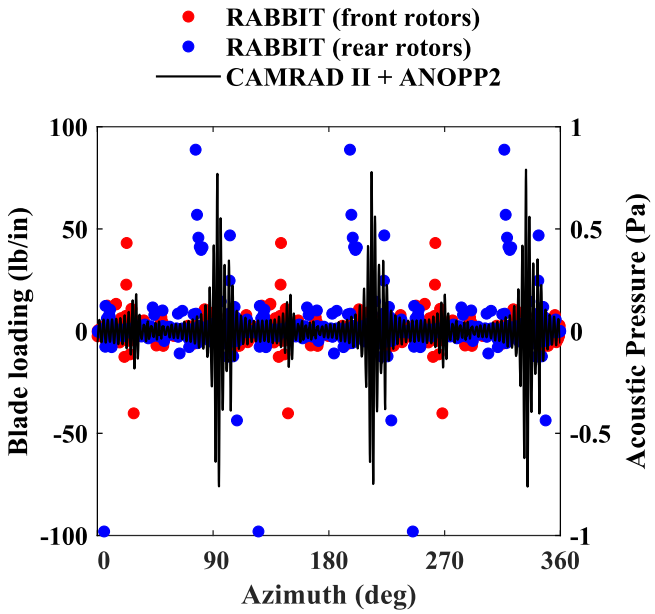

Figure 14. RABBIT and CAMRAD II + ANOPP2 predictions NASA RVLT Conceptual design quadrotor.

To highlight RABBITs capability, another quadrotor rotor case was run with the same flight conditions as shown in Table 3, but with the rear rotors set 0.11 R below the front rotors, to ensure rotor-rotor wake interaction would occur. The two quadrotor cases are compared and shown in Fig. 15 a) for a rear rotor baseline height of 0.35 R and b) for a rear rotor height of -0.11 R. The rear rotor height of -0.11 R reveals additional BVI occurrences compared to the 0.35 R rear rotors. A visual rendering of the quadrotor with a rear rotor height of -0.11 R is shown in Fig. 16. a) reveals that a rear rotor height of -0.11 R is placed in the path of the front rotors wakes, which results in the front rotors wakes to hit the rear. A zoomed in visualization of a BVI occurrence is shown in Fig. 16 b), where one of the front rotor blade vortices (magenta pink) hits a rear rotor blade (yellow).

The current change of rotor blade loading within RABBIT does not account for aging vortex characteristics which is why a BVI occurrence from a vortex shed from the front rotors hitting the back rotors is just as intense as if the vortex travelled a lesser distance. Improvements to the BVI Impulse Function to account for wake age could improve the fidelity of these predicted BVI events.

a)

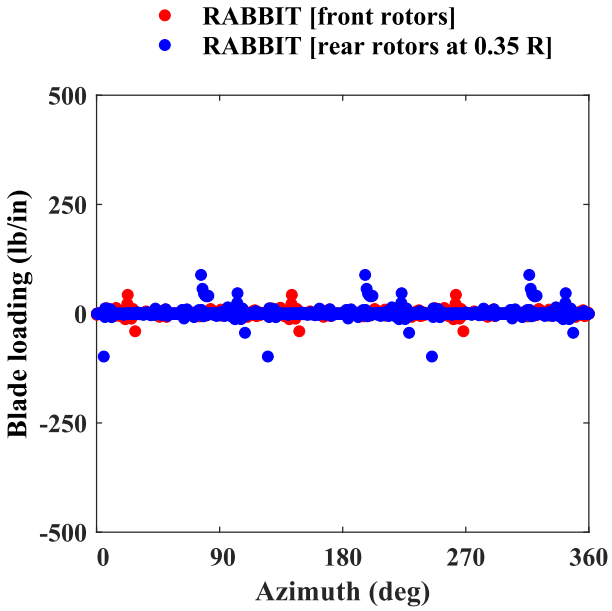

b)

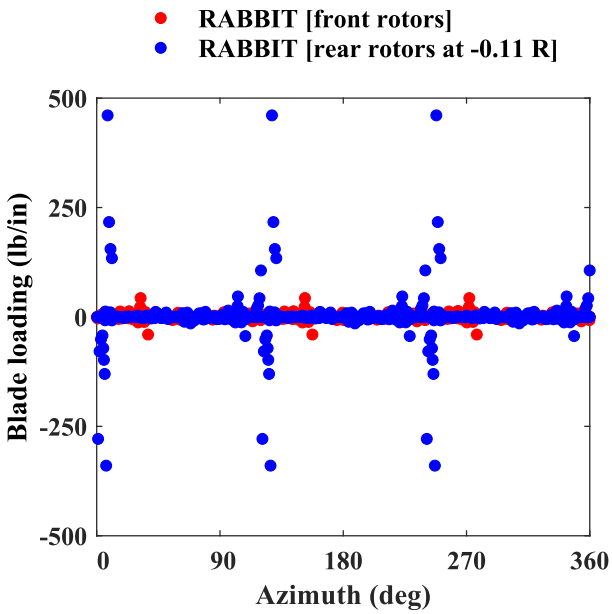

Figure 15. RABBIT predictions NASA RVLT Conceptual design quadrotor comparing rear rotor heights of a) 0.35 R and b) -0.11 R.

a)

b)

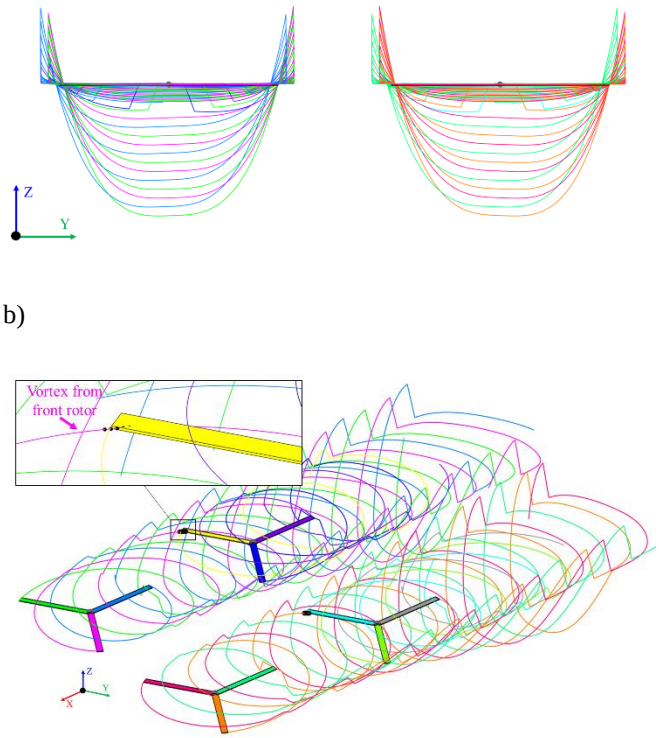

Figure 16. NASA RVLT Conceptual design quadrotor at 0.11 R rear rotor height a) RABBIT simulation Y-Z plane view and b) visual rendering highlighting rear BVI occurrence from a front rotor blade vortex.

CONCLUSIONS

The low fidelity RABBIT tool has been further upgraded to enable engineers to quickly design and simulate UAM configurations and assess BVI occurrence for a desired flight condition. To highlight RABBIT's improvements and capabilities, the Lopes rotor and the NASA RVLT Quadrotor were simulated along with providing acoustic predictions from CAMRAD II and ANOPP2 to further validate RABBIT's capabilities against a mid-fidelity comprehensive analysis tool by highlighting BVI location and strength.

Improvements to RABBIT's algorithm include decreasing computational time, accounting for BVI source time arrival of desired observer location, improving vortex strength modeling to account for thrust, rotational speed, and chord, and enhancing the BVI impulse factor formulation. A study was performed to aid in selecting appropriate RABBIT specific parameters including rotation length, wake resolution, wake age length, and BVI tolerance factor. Along with this study, best practices were provided to ensure the user properly selects the appropriate values for each of these parameters. Finally, the use of MATLAB's App Designer has enabled RABBIT to reach a broader audience with its user interface.

FUTURE WORK

RABBIT can further be enhanced to incorporate abilities to further improve ease of use and increase fidelity. A brief list of possible future improvements include:

- Improve blade loading formulation to account for wake age to capture ageing vortex characteristics
- Include Mach number/radiation cone principle to consider BVI noise directivity for a given microphone location
- Implementation of Farrasaats Formulation 1A to predict thickenss and loading terms (Ref. 13) and also inlcude broadband noise prediction model (Ref. 14)
- Implement higher fidelity wake models to capture higher order aerodynamic effects
- Output text file that includes a list of all assumptions used for simulation
- Option to switch between English and metric units.
- Ability to export various forms of images beyond Portable Network Graphics
- Capability to import rotor geometry .stl files and complex rotor geometry builder to include twist, taper, and more
- Streamline coupling with comprehensive analysis tools
- Further improve user interface by conducting beta tests for various educational levels of engineers

AUTHOR CONTACT INFORMATION

Natasha Schatzman Natasha.Schatzman@nasa.gov
Kevin Holly Kevinh@mathworks.com

ACKNOWLEDGMENTS

Thank you to the NASA's Revolutionary Vertical Lift Technology (RVLT) project and MathWorks for their support. Thank you to Doug Boyd and Wayne Johnson for valuable technical input and discussion. A huge thank you to Ethan Romander, Benny Cheung, Lauren Weist, and Jason Cornelius.

All of this work could not have been done without the support from the late Ben Sim.

REFERENCES

1. Johnson, W., "CAMRAD II Comprehensive Analytical Model of Rotorcraft Aerodynamics and Dynamics," Johnson Aeronautics, Palo Alto, CA, 2005.
2. Lopes, L. V., and Burley, C. L., "Design of the Next Generation Aircraft Noise Prediction Program: ANOPP2," 17th AIAA/CEAS Aeroacoustics Conference Proceedings, Portland, OR, June 2011. DOI: 10.2514/6.2011- 2854.

3. Schatzman, N. L., “Aerodynamics and Aeroacoustic Sources of a Coaxial Rotor,” NASA TM 219895, April 2018.
4. Sim, B. W., and George, A. R., “Development of a Rotor Aerodynamic Load Prediction Scheme for Blade-Vortex Interaction Noise Study,” American Helicopter Society 51st Annual Forum, Fort Worth, TX, March 1995.
5. Beddoes, T. S., “A Wake Model for High Resolution Airloads,” Proceedings of the 2nd International Conference on Basic Rotorcraft Research, University of Maryland, College Park, MD, 1985.
6. Ringler, T. D. , George, A. R. and Steele, J. B. , “The Study of Blade-Vortex Interaction Sound Generation and Directionality, " Proceedings of the AHS Technical Specialist Meeting, October 1991.
7. Silva, C. and Johnson, W., “Practical Conceptual Design of Quieter Urban VTOL Aircraft,” Vertical Flight Society’s 77th Annual Forum and Technology Display, Virtual, April 2021.
8. Weist, L., and Schatzman, N., "RABBIT: A Rapid Low Fidelity BVI Prediction Tool—Comparison and Validation using the NASA RVLT Toolchain," Presented at the VFS Aeromechanics for Advanced Vertical Flight Technical Meeting, San Jose, CA, Jan 25-27, 2022.
9. Weist, L., Schatzman, N. L., and Shirazi, D., “Best Practices for Predicting Acoustics of a Single Rotor Using the NASA RVLT Conceptual Design Toolchain”, To be presented at The Transformative Vertical Flight Conference, Santa Clara, CA, February 6-8, 2024.
10. MATLAB, version 9.14.0.2206163 (R2023a), The MathWorks Inc., Natick, Massachusetts, 2010.
11. Leishman, J. G., *Principles of Helicopter Aerodynamics*, New York, NY, Cambridge University Press, 2000.
12. Systems Analysis and Concepts Directorate, “NASA Urban Air Mobility (UAM) Reference Vehicles,” NASA, dated September 2,2023, https://sacd.larc.nasa.gov/uam-refs/ (accessed December 1, 2023).
13. Brentner, Kenneth S., “Prediction of Helicopter Discrete Frequency Rotor Noise- A Computer Program Incorporating Realistic Blade Motions and Advanced Formulation”, NASA TM 87721, October 1986.
14. Brooks, T.F., Pope, D.S. and Marcolini, M.A., “Airfoil Self-Noise and Prediction,” NASA RP 1218, July 1989.